Kai Volgmann*, Alexander Schulz, Anna-Maria Welsch, Thomas Bredow, Suliman Nakhal, Martin Lerch, and Paul Heitjans

Lattice Vibrations to Identify the Li/Na Ratio in $Li_xNa_{2-x}Ti_6O_{13}$ ($x = 0 \ldots 2$)

DOI 10.1515/zpch-2015-0585
Received February 24, 2015; accepted August 5, 2015

Abstract: $Li_xNa_{2-x}Ti_6O_{13}$ has received attention as 3*d*-metal oxide based anode material for possible battery application. Generally, titanium oxides represent excellent Li hosts due to their zero-strain behavior, cycling stability and high operating voltage. New developments choose Na as charge carrier, but less effort is put in the investigation of mixed cation conductors. Owing to the synthesis route of $Li_xNa_{2-x}Ti_6O_{13}$ ($0 \le x \le 2$) the coordination of Na and Li in the channels is different which had been investigated by means of X-ray and neutron diffraction. Up to now, no Raman spectroscopy has been applied. This oxide is highly Raman-active, thus the local structure can also be analyzed in terms of vibrational spectroscopy. Micro-Raman spectroscopy carried out at room temperature with different cation contents ($x = 0, 0.33, 1, 2$) shows the continuous change from Na to Li by a superposition of the modes for $Na_2Ti_6O_{13}$ and $Li_2Ti_6O_{13}$. The only exceptions are two distinct modes. They appear either for Li (118 cm^{-1}) or Na (135 cm^{-1}). The results confirm the high-temperature phase stability of $Na_2Ti_6O_{13}$ as well as the anisotropic thermal expansion of the unit cell seen by *in situ* X-ray powder diffrac-

***Corresponding author: Kai Volgmann,** Institute of Physical Chemistry and Electrochemistry; and ZFM – Center for Solid State Chemistry and New Materials, Leibniz Universität Hannover, Callinstr. 3–3a, 30167 Hannover, Germany, e-mail: volgmann@pci.uni-hannover.de
Alexander Schulz, Paul Heitjans: Institute of Physical Chemistry and Electrochemistry; and ZFM – Center for Solid State Chemistry and New Materials, Leibniz Universität Hannover, Callinstr. 3–3a, 30167 Hannover, Germany
Anna-Maria Welsch: Institute of Mineralogy, Leibniz Universität Hannover, Callinstr. 3, 30167 Hannover, Germany; and ZFM – Center for Solid State Chemistry and New Materials, Leibniz Universität Hannover, Callinstr. 3–3a, 30167 Hannover, Germany
Thomas Bredow: Mulliken Center for Theoretical Chemistry, Institut für Physikalische und Theoretische Chemie, Universität Bonn, Beringstr. 4, 53115 Bonn, Germany; and ZFM – Center for Solid State Chemistry and New Materials, Leibniz Universität Hannover, Callinstr. 3–3a, 30167 Hannover, Germany
Suliman Nakhal, Martin Lerch: Institut für Chemie, Sekr. C2, Technische Universität Berlin, Straße des 17. Juni 135, 10623 Berlin, Germany

tion under two different gas atmospheres. Combining these results, we suppose that the anisotropic thermal expansion of the lattice parameters is affected by the normal vectors of the corresponding bond vibrations in $Na_2Ti_6O_{13}$ and $Li_2Ti_6O_{13}$. Crystalline-orbital calculations of the Raman shifts of $Li_xNa_{2-x}Ti_6O_{13}$ were carried out for the cation contents $x = 0, 1, 2$ and Raman modes were assigned to specific bond vibrations supported by theory. Besides, this gives additionally information about the Li/Na ratio in a new and simple way.

Keywords: *In situ* X-ray Diffraction, X-ray Diffraction Analysis, Raman Spectroscopy, $Na_2Ti_6O_{13}$, $Li_2Ti_6O_{13}$, Mixed Cation Conductor.

1 Introduction

Lithium titanium oxides are of special interest as they exhibit properties suitable for application as Li ion battery anode materials [1]. Those properties are, e.g., zero-strain behavior and cycling stability. Especially TiO_2 has been under investigation as it is the most promising candidate besides $Li_4Ti_5O_{12}$. Apart from the spinel ($Li_4Ti_5O_{12}$) [1, 2] and the layered structure (orthorhombic $Li_2Ti_3O_7$) [3], alkali titanates can exhibit channel structure which applies to monoclinic $Li_xNa_{2-x}Ti_6O_{13}$ being of interest here. Due to its structural properties, this compound is also attractive for fundamental diffusion studies as performed by us on various Li ion conductors [4–7]. Another topic is the change of the cation, i.e. turning to sodium [8]. For example, TiO_2 or $Na_2Ti_3O_7$ seem to be excellent candidates as Na hosts [9, 10]. What has not been considered in the system $Li_xNa_{2-x}Ti_6O_{13}$ up to now is the influence of the mixing of these two cations on their diffusivity (mixed alkali effect, see e.g. [11]). To investigate the ionic conductivity and structural properties with different Li/Na content ratios in titanium oxides, $Li_xNa_{2-x}Ti_6O_{13}$ proves useful as we not only have an electronic insulator but can also tune the cation ratio via an ion exchange synthesis. In this study, we mainly focus on structural properties influenced by the cation (content) ratio. As X-ray and neutron diffraction data are widely known from the literature [12, 13], we confine ourselves to additional *in situ* X-ray powder diffraction (XRPD) measurements at higher temperatures for $Na_2Ti_6O_{13}$ under argon and synthetic air gas atmospheres. Moreover, we use micro-Raman spectroscopy as a method to identify the Li/Na ratio in $Li_xNa_{2-x}Ti_6O_{13}$. This is analogous to, e.g., the identification of the Li/Si ratio in lithium silicate glasses [14, 15]. To our knowledge, this has not been done for the alkali metal ratio in titanates. Structural details were also analyzed and compared to XRPD results, as, e.g., in [6]. The Raman spec-

troscopy results are supported by theoretical calculations of the Raman modes for $Na_2Ti_6O_{13}$ and $Li_2Ti_6O_{13}$ using the program package CRYSTAL14 [16].

2 Experimental and Theoretical Details

Solid-state synthesis of $Na_2Ti_6O_{13}$ was conducted as published in the literature [12, 17]. Stoichiometric amounts of Na_2CO_3 and TiO_2 were mixed and ground in a mortar. The powder was filled in Al_2O_3 crucibles and a two-step temperature program was carried out. First, the powder was heated to 1073 K for 16 h for decomposition of the carbonate. Second, the powder was reground and pelletized and heated to 1273 K for 24 h. After synthesis, X-ray powder diffraction verified phase-pure $Na_2Ti_6O_{13}$. In a subsequent step, an ion exchange reaction using molten $LiNO_3$ was employed to achieve a particular Li/Na ratio and the complete removal of Na and insertion of lithium. Complete Na removal was achieved as described in [17]. $LiNO_3$ and $Na_2Ti_6O_{13}$ were mixed in equal stoichiometric amounts with a 150% excess of $LiNO_3$ to compensate the loss of Li. The mixture was held at a temperature of 598 K for 4 days. To achieve Li contents of $x = 0.33$ and $x = 1$, the time for the ion exchange was reduced to 24 h and 48 h, respectively. The products were ground a second time and washed with ethanol after ion exchange. XRPD measurements confirmed single phase $Li_xNa_{2-x}Ti_6O_{13}$ again. The lithium content was checked using inductively coupled plasma optical emission spectroscopy (ICP-OES). The setup consists of a Varian ICP-OES 715 and a microwave oven MLS START 1500. A small amount of the product was weighted in a PTFE beaker. Pulping was done using HNO_3.

In situ XRPD was carried out on a D8 Advance Diffractometer (Bruker AXS) with Bragg-Brentano geometry (θ/θ) using Cu K$\alpha_{1,2}$ ($\lambda = 0.154$ nm) radiation, secondary Ni-filter and a one-dimensional LynxEye detector (silicon strip). The XRPD measurements of $Na_2Ti_6O_{13}$ were performed between 10° and 100° (2θ), step size 0.01°, time per step 0.27 s and a total number of 8557 steps. The samples were not rotated during measurement. A high-temperature cell HTK 1200N by Anton Paar GmbH was used. The temperature range chosen for *in situ* XRPD was 300 K to 1300 K for both Ar atmosphere and synthetic air (free of hydrocarbons). The XRD patterns were analyzed using the software TOPAS v4.2 for Rietveld analysis. A Chebyshev polynomial was applied for background correction. Peak shapes were fitted using the pseudo-Voigt Thompson-Cox-Hastings profile function (PV-TCHZ) [18]. Start values for refinement were taken from [19].

Raman spectroscopy was carried out using a micro-Raman spectrometer (Bruker Senterra). For all measurements a laser with a wavelength of $\lambda = 532$ nm

(depolarized beam) and a power of 10 mW was applied. A 50× objective lens was used for focusing. Before each measurement, a calibration using a silicon standard was done. The range of 50–1555 cm^{-1} was observed with a spectral resolution of 3–5 cm^{-1}. An integration time of 2 s per point was used and 10 spectra were accumulated. Powder samples were prepared and measured under normal air atmosphere at room temperature. The spectra have been temperature-corrected for Bose-Einstein occupational factor [20, 21]. For better clarity the spectra have been additionally integrated over the area between 70–1000 cm^{-1} and scaled.

For an analysis of the Raman modes, theoretical calculations were performed for $Na_2Ti_6O_{13}$, $LiNaTi_6O_{13}$ and $Li_2Ti_6O_{13}$ using the crystalline-orbital program package CRYSTAL14 [16]. Vibration modes were calculated applying numerical force constant matrix calculations as described in [22]. Raman intensities were obtained from the recently implemented Coupled-Perturbed Kohn-Sham (CPKS) scheme [23, 24]. In order to match the experimental conditions, a temperature of 300 K and a laser excitation wavelength of 532 nm was used in the intensity calculations. Standard basis sets of triple-zeta (Ti) and triple-zeta plus polarization (Na, Li, O) quality were taken from the CRYSTAL website [25]. The generalized gradient approximation (GGA) functional according to Perdew, Burke and Ernzerhof (PBE) [26] was applied as it has provided accurate results for spectroscopic properties in a previous study [27] and has been tested for Raman intensities in CRYSTAL14. For $Li_2Ti_6O_{13}$ and $Na_2Ti_6O_{13}$ the crystal lattice parameters for calculation were taken from experiment [13] and kept fixed while the atomic positions were fully relaxed in order to obtain a stationary point for the vibration analysis. For calculations of the mixed compound $LiNaTi_6O_{13}$ also the lattice parameters were optimized. Three different structure models were generated for this compound, two were created from the unit cells of the end members $Li_2Ti_6O_{13}$ and $Na_2Ti_6O_{13}$ by substituting one Li (Na) by Na (Li). The third model is based on $Na_2Ti_6O_{13}$ where one Na atom is removed and a Li atom is placed on a fourfold coordinated site. Integral tolerances were set to rather strict values (7, 7, 7, 7, 14) in order to diminish numerical noise in the numerical evaluation of the Hessian. A 4 × 4 × 4 Monkhorst–Pack grid was used for integration in reciprocal space.

3 Results

In situ XRPD for $Na_2Ti_6O_{13}$ was performed under Ar and synthetic air atmosphere as well as for an extended temperature range up to 1300 K to check for phase stability under these conditions. Figure 1 shows the plot of XRPD patterns for selected temperatures. No additional reflections are observed throughout the whole tem-

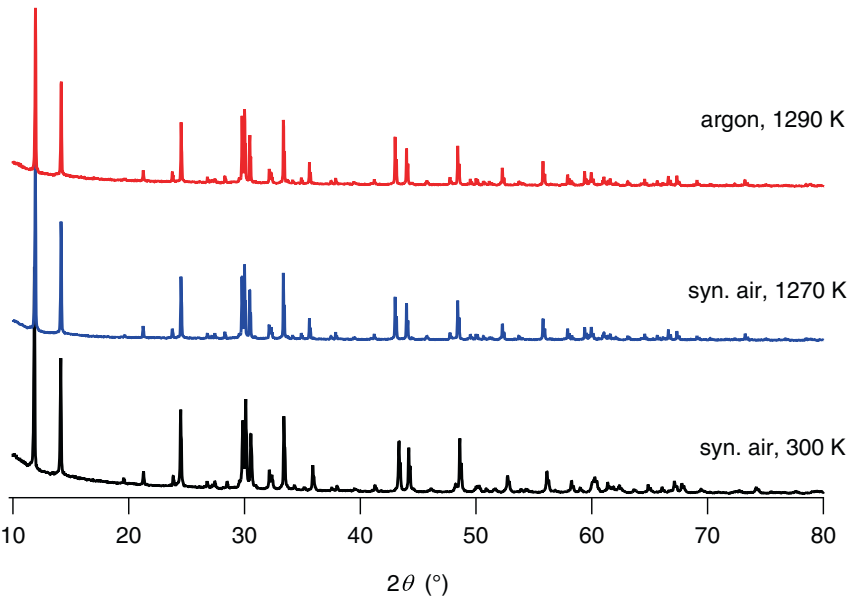

Figure 1: *In situ* XRD patterns of $Na_2Ti_6O_{13}$ in synthetic air and argon. Measurements in both atmospheres show no phase change or additional reflections over the complete temperature range.

perature range. Only a shift in 2θ due to the thermal expansion is visible. The same phase stability has also been observed in Argon atmosphere as can be deduced from the lattice parameters. In Figure 2 and Table 1 the results of the Rietveld analyses are shown. For all three lattice parameters, the thermal expansion increases with increasing temperature. As already discussed in [13] for $Li_2Ti_6O_{13}$, the a and c lattice parameters show also a non-linear thermal expansion for $Na_2Ti_6O_{13}$. This effect increases slightly if the temperature is raised above 700 K. The lattice parameter b shows a constant linear slope in the range 300–1300 K.

Raman spectroscopy results are presented in Figure 3. It is an overview for all Li/Na ratios ($x = 0, 0.33, 1, 2$). From the space group *C 2/m*, the kind of possible active Raman modes can already be derived. A_g and B_g modes are possible modes and transitions between both modes are allowed [28]. As we use Raman spectroscopy as a method sensitive to lattice vibrations, we devide the spectra into two regions. The region 70–350 cm^{-1} is mostly sensitive to vibrations of cation–oxygen bonds. Towards higher energies in the region 350–1000 cm^{-1}, vibrations mainly of TiO_6 octahedra were found comparable to NbO_6 units in $LiNbO_3$ [29, 30]. The vibrations of these octahedra show only small Raman shifts due to cation exchange. If compared to other mixed cation compounds, the lattice

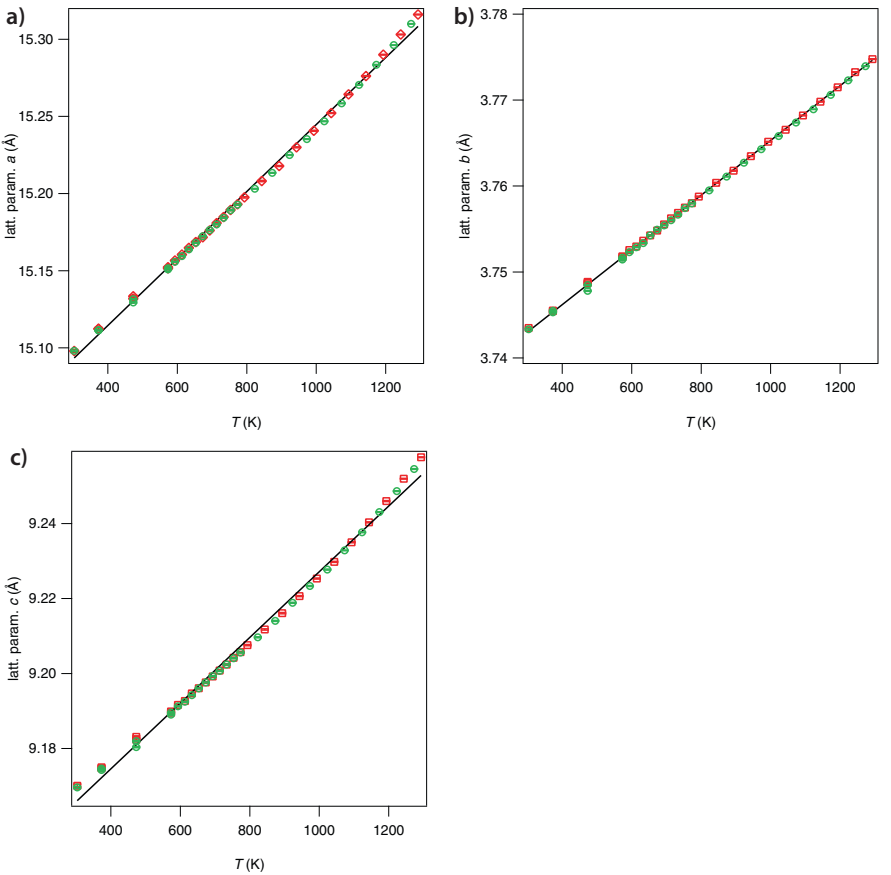

Figure 2: Results of the Rietveld refinements using DIFFRACplus TOPAS v4.2. Lattice parameters *a*, *b* and *c* are shown for both gas atmospheres (red squares: argon, green circles: synthetic air). The parameters *a* and *c* show a non-linear thermal expansion (Figs. 2a and c). A change in slope can be observed around 700 K for these parameters whereas the lattice parameter *b* keeps linear over the whole temperature range (Fig 2b). The straight black lines demonstrate the non-linear thermal expansion of the lattice parameters in Figs. 2a and c.

framework is often not affected by such an exchange [31, 32]. Thus, for a detailed analysis of the Li/Na ratio, the spectral region up to 350 cm^{-1} seems to be the best choice for a qualitative distinction. A continuous change in the Raman shifts as function of the Li/Na ratio can be observed in Figure 3. Some Raman modes of $Na_2Ti_6O_{13}$ disappear whereas new shifted signals for $Li_2Ti_6O_{13}$ appear in the intermediate range. According to the relative shift of a single mode and the assign-

Table 1: Results of Rietveld refinements for several temperatures and argon **(a)** and synthetic air **(b)** atmospheres. Rietveld refinements were carried out using DIFFRACplus TOPAS v4.2 software.

	300 K	470 K	670 K	890 K	1290 K
(a)					
$x*$	0.4657(15)	0.4653(10)	0.4668(8)	0.4671(7)	0.4671(7)
$y*$	0	0	0	0	0
$z*$	0.2726(23)	0.2665(15)	0.2653(12)	0.2654(11)	0.2693(11)
Na occupancy	0.973(27)	0.918(16)	0.901(13)	0.856(11)	0.841(11)
a / Å	15.0980(11)	15.1336(6)	15.1718(5)	15.2179(3)	15.3160(2)
b / Å	3.74350(15)	3.74883(9)	3.75490(7)	3.76179(5)	3.77477(4)
c / Å	9.1701(4)	9.1831(3)	9.1977(2)	9.2161(2)	9.2577(1)
V / Å^3	511.869(50)	514.394(28)	517.237(21)	520.694(16)	528.056(11)
β / °	99.0242(38)	99.1244(22)	99.2032(16)	99.2736(13)	99.3905(9)
R_p	7.40	7.00	6.96	6.91	7.53
R_{exp}	9.50	8.39	7.84	7.52	7.23
R_{wp}	9.83	9.24	9.08	8.99	9.67
GOF	1.04	1.10	1.16	1.20	1.34
R Bragg	2.63	3.67	4.06	4.39	6.46
(b)					
$x*$	0.4628(5)	0.4638(6)	0.4639(5)	0.4641(5)	0.4651(6)
$y*$	0	0	0	0	0
$z*$	0.2650(7)	0.2649(8)	0.2658(8)	0.2655(9)	0.2674(9)
Na occupancy	1.000(8)	0.890(9)	0.855(8)	0.829(8)	0.763(9)
a / Å	15.0981(5)	15.1294(4)	15.1723(3)	15.2135(3)	15.3100(2)
b / Å	3.74334(11)	3.74774(6)	3.75492(5)	3.76110(4)	3.77394(3)
c / Å	9.16962(28)	9.18036(16)	9.19764(13)	9.21405(13)	9.25456(9)
V / Å^3	511.825(28)	513.955(18)	517.245(14)	520.336(13)	527.5618(93)
β / °	99.0250(13)	99.1197(14)	99.2067(11)	99.2697(10)	99.3848(7)
R_p	6.00	6.73	6.72	6.95	7.58
R_{exp}	5.28	5.26	5.43	5.49	5.59
R_{wp}	7.77	8.65	8.49	8.87	9.46
GOF	1.47	1.64	1.56	1.62	1.69
R Bragg	3.78	3.57	4.36	4.77	6.14

* Only Na atom positions

ment of modes only present in $Na_2Ti_6O_{13}$ or $Li_2Ti_6O_{13}$ qualitative information on the Li/Na ratio can be given as it is shown now with the aid of calculations.

Figure 4 shows the theoretical prediction of Raman modes for $Na_2Ti_6O_{13}$ (Figure 4a) and $Li_2Ti_6O_{13}$ (Figure 4b) in comparison with the experiment. Despite a small offset in wave numbers, the assignment of all experimental modes is possible. The calculated intensities match if signal ratios are compared. The devia-

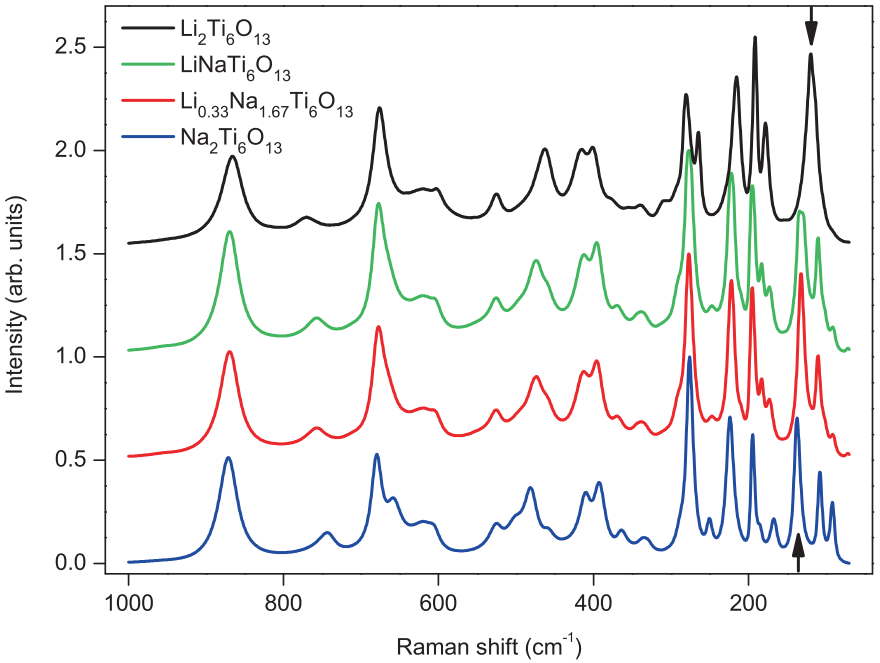

Figure 3: Raman shifts measured for $Li_xNa_{2-x}Ti_6O_{13}$ ($x = 0, 0.33, 1, 2$) at room temperature. Laser wavelength $\lambda = 532\,nm$, spectral range measured $50–1550\,cm^{-1}$. The region shown is $70–1000\,cm^{-1}$ as no signals are observed outside this range. The low-energy region ($70–350\,cm^{-1}$) shows mainly modes affected by vibrations of cation–oxygen bonds. Thus, it is sensitive to the Li/Na ratio. For $Na_2Ti_6O_{13}$ a mode at $135\,cm^{-1}$ and for $Li_2Ti_6O_{13}$ a mode at $118\,cm^{-1}$ are observed. Both modes are indicated with an arrow.

tions between theory and experiment are in the range observed for other compounds in a previous study on $Na_8[AlSiO_4]_6(BH_4)_2$ [27]. Small deviations could arise from the fact that a powder is measured and its surface is not perfectly plain. Thus, some Raman intensities are scattered more than others. As a perfect polycrystalline solid is simulated, the influence of defects is not considered in the calculation. Both can lead to a mismatch in calculated and experimental Raman intensities.

Besides these limitations, there are particular features for both $Na_2Ti_6O_{13}$ and $Li_2Ti_6O_{13}$. Most experimental and calculated modes are present in both compounds. But there is an intense bond vibration of the Na in $Na_2Ti_6O_{13}$ which appears at $135\,cm^{-1}$. This signal disappears in $Li_2Ti_6O_{13}$ where a new strong signal arises at $118\,cm^{-1}$ (calculated $111\,cm^{-1}$). This pair helps in differentiating between the two compounds as the other contributions are found in both. In

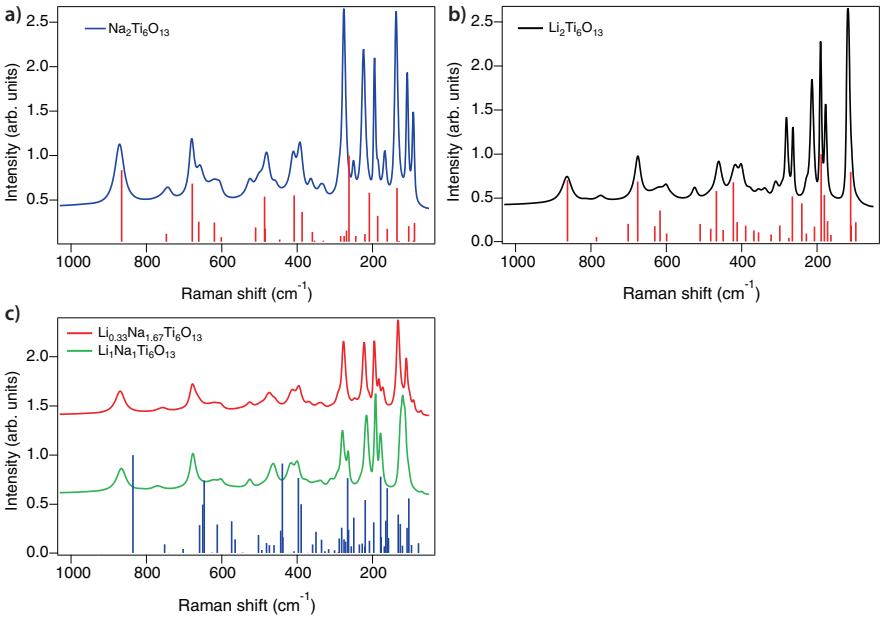

Figure 4: Comparison of experimental and calculated Raman shifts for $Na_2Ti_6O_{13}$ (Fig. 4a), $Li_2Ti_6O_{13}$ (Fig. 4b), $Li_{0.33}Na_{1.67}Ti_6O_{13}$ and $LiNaTi_6O_{13}$ (Fig. 4c). Total intensities calculated by CRYSTAL14 are shown for a polycrystalline material as the experimental spectrum is recorded for a powder. Calculated intensities are scaled for better visibility of contributions with low intensity. For $LiNaTi_6O_{13}$, the calculation started from $Li_2Ti_6O_{13}$ by replacing one Li atom by a Na atom at the same site.

$Li_{0.03}Na_{0.97}Ta_{0.4}Nb_{0.6}O_3$, similar modes for Na (142 cm^{-1}) and Li (118 cm^{-1}) are observed [32].

Calculating the Raman shifts for $Li_xNa_{2-x}Ti_6O_{13}$ also helps in understanding the anisotropic thermal expansion. As mentioned above, our *in situ* XRPD results for $Na_2Ti_6O_{13}$ show the same thermal evolution of the lattice parameters as in $Li_2Ti_6O_{13}$. This leads to the assumption that independent of the cation ratio, the lattice parameters *a* and *c* are more affected. Raman spectroscopy and the corresponding calculations let us suppose that the normal vectors of the bond vibrations in these directions have an effect on the anisotropic expansion.

Furthermore, Figure 4c shows the calculation for a Li/Na ratio equal to 1. Compared to $Li_{0.33}Na_{1.67}Ti_6O_{13}$, the calculation does not match well and the prediction for $Na_2Ti_6O_{13}$ fits the experiment better. If the experimental data for $LiNaTi_6O_{13}$ is compared, the results match better. This is true for starting the calculation at $Li_2Ti_6O_{13}$ and replacing one Li with Na on a 4*i* position. For this arrangement, the Na moves to its 8-fold coordination as in $Na_2Ti_6O_{13}$ [13].

The mixed cation compound in general shows the sum of the Raman modes for $Na_2Ti_6O_{13}$ and $Li_2Ti_6O_{13}$. The modes at ≈ 75 cm^{-1} and at ≈ 560 cm^{-1} are shifted in $Li_1Na_1Ti_6O_{13}$. These may point to a specific bond vibration in this mixed cation compound.

4 Discussion

In addition to literature results, our *in situ* XRPD measurements show a phase stability of $Na_2Ti_6O_{13}$ up to 1300 K both in Ar and synthetic air atmosphere. This is quite surprising as at least in a reducing environment a removal of oxygen could have been expected and as a consequence a breakdown of the lattice stability might have been supposed as it is the case for $Li_2Ti_6O_{13}$ [12]. This has not been observed in the chosen temperature range. With increasing temperature, a non-linear increase of the lattice parameters *a* and *c* has been found for $Na_2Ti_6O_{13}$ as in the case of $Li_2Ti_6O_{13}$ [13]. This could be attributed to stronger lattice vibrations due to a minimal shift in the sodium position. As Pérez-Flores et al. stated in [13], they attribute the stronger increase of the lattice parameters *a* and *c* to the shift of the Li to a four-fold coordination in $Li_2Ti_6O_{13}$ instead of an eight-fold coordination in $Na_2Ti_6O_{13}$. This lower coordination may favor a higher vibrational movement of the Li-O bonds. As we also see this effect in $Na_2Ti_6O_{13}$, the change in coordination is an argument for two different vibrational modes in Raman spectra for either Li or Na. But we additionally suppose that the anisotropic thermal expansion of the lattice parameters is affected by the normal vectors of the corresponding bond vibrations in both $Na_2Ti_6O_{13}$ and $Li_2Ti_6O_{13}$.Thus, mostly independent of the cation coordination both Na–O and Li–O bond vibrations lead to an anisotropic thermal expansion. Its strength depends on the kind of cation.

The Raman spectroscopy results could help answering further questions as we observe distinct modes for either Na (135 cm^{-1}) or Li (118 cm^{-1}) in $Li_xNa_{2-x}Ti_6O_{13}$. This enables us to qualitatively distinguish between the various Li/Na ratios. In the mixed cation compounds, some additional and shifted modes point to a small influence on these octahedra. If both Li and Na are neighboured, this leads to a distortion of the lattice as observed through the shift of Raman modes at 75 cm^{-1} and 560 cm^{-1}. Owing to this observation also an interaction of both cations can be supposed.

5 Conclusions

Both for Na and Li distinct Raman modes were observed, whereas for the different Li/Na content ratios shifted and additional modes showed up pointing to a small distortion of the TiO_6 octahedra vibrations. The best prediction of the experimental spectrum of $LiNaTi_6O_{13}$ was achieved by replacing Li with Na in $Li_2Ti_6O_{13}$. The calculated normal vectors lead to the assumption that lattice vibrations cause the anisotropic thermal expansion of the lattice parameters *a* and *c* which was also observed in our *in situ* XRD measurements of $Na_2Ti_6O_{13}$. The combination of these techniques provides additional information on structural properties. Our study shows that Raman spectroscopy can be a versatile tool in studying the structural properties of battery materials. The amount of insertion or the ratio of cation contents can be qualitatively determined.

Acknowledgement: We thank the workgroup of Prof. Caro (Hannover) for access to the X-ray diffractometer. Financial support by the DFG in the frame of the Research Unit FOR 1277 (molife) is gratefully acknowledged.

References

1. G.-N. Zhu, Y.-G. Wang, and Y.-Y. Xia, Energy Environ. Sci. **5** (2012) 6652.
2. X. Sun, P. V. Radovanovic, and B. Cui, New J. Chem. **39** (2014) 38.
3. K. Chiba, N. Kijima, Y. Takahashi, Y. Idemoto, and J. Akimoto, Solid State Ionics **178** (2008) 1725.
4. P. Heitjans, S. Indris, and M. Wilkening, Diffus. Fundam. **2** (2005) 45.1.
5. A. Kuhn, M. Kunze, P. Sreeraj, H. D. Wiemhöfer, V. Thangadurai, M. Wilkening, and P. Heitjans, Solid State Nucl. Magn. Reson. **42** (2012) 2.
6. P. Heitjans, M. Masoud, A. Feldhoff, and M. Wilkening, Faraday Discuss. **134** (2006) 67.
7. B. Ruprecht, M. Wilkening, R. Uecker, and P. Heitjans, Phys. Chem. Chem. Phys. **14** (2012) 11974.
8. A. Rudola, K. Saravanan, S. Devaraj, H. Gong, and P. Balaya, Chem. Commun. **49** (2013) 7451.
9. L. Wu, D. Buchholz, D. Bresser, L. Chagas Gomes, and S. Passerini, J. Power Sources **251** (2014) 379.
10. P. Senguttuvan, G. Rousse, V. Seznec, J.-M. Tarascon, and M. Palacín, Chem. Mater. **23** (2011) 4109.
11. A. Bunde, W. Dieterich, P. Maass, and M. Meyer, in: P. Heitjans and J. Kärger (Eds.), *Diffusion in Condensed Matter: Methods, Materials, Models*, Springer, Berlin and New York, pp. 813–856, (2005).
12. K. Kataoka, J. Awaka, N. Kijima, H. Hayakawa, K.-I. Ohshima, and J. Akimoto, Chem. Mater. **23** (2011) 2344.

13. J. C. Pérez- Flores, C. Baehtz, M. Hoelzel, A. Kuhn, and F. García-Alvarado, Phys. Chem. Chem. Phys. **14** (2012) 2892.
14. A.-M. Welsch, H. Behrens, I. Horn, S. Ross, and P. Heitjans, J. Phys. Chem. A **116** (2012) 309.
15. U. Bauer, A.-M. Welsch, H. Behrens, J. Rahn, H. Schmidt, and I. Horn, J. Phys. Chem. B **117** (2013) 15184.
16. R. Dovesi, R. Orlando, A. Erba, C. M. Zicovich- Wilson, B. Civalleri„ S. Casassa, L. Maschio, M. Ferrabone, M. La Pierre De, P. D'Arco, Y. Noël, M. Causà, M. Rérat, and B. Kirtman, Int. J. Quantum Chem. **114** (2014) 1287.
17. J. C. Pérez-Flores, A. Kuhn, and F. García-Alvarado, J. Power Sources **196** (2011) 1378.
18. R. A. Young, *The Rietveld method, International Union of Crystallography*, Oxford University Press, [Chester, England], Oxford, New York, (1993).
19. S. Andersson and A. D. Wadsley, Acta Cryst. **15** (1962) 194.
20. M. Hass, Solid State Commun. **7** (1969) 1069.
21. R. Shuker and R. W. Gammon, Phys. Rev. Lett. **25** (1970) 222.
22. F. Pascale, C. M. Zicovich-Wilson, F. López Gejo, B. Civalleri, R. Orlando, and R. Dovesi, J. Comput. Chem. **25** (2004) 888.
23. M. Ferrero, M. Rérat, R. Orlando, and R. Dovesi, J. Comput. Chem. **29** (2008) 1450.
24. L. Maschio, B. Kirtman, M. Rérat, R. Orlando, and R. Dovesi, J. Chem. Phys. **139** (2013) 164102.
25. http://www.crystal.unito.it/basis-sets.php, accessed 8 January 2015.
26. J. P. Perdew, K. Burke, and M. Ernzerhof, Phys. Rev. Lett. **77** (1996) 3865.
27. A. G. Schneider, T. Bredow, L. Schomborg, and C. H. Rüscher, J. Phys. Chem. A **118** (2014) 7066.
28. M. I. Aroyo, A. Kirov, C. Capillas, J. M. Perez-Mato, and H. Wondratschek, Acta Cryst. A **62** (2006) 115.
29. S. D. Ross, J. Phys. C: Solid State Phys. **3** (1970) 1785.
30. R. F. Schaufele and M. J. Weber, Phys. Rev. **152** (1966) 705.
31. N. V. Sidorov, M. N. Palatnikov, N. A. Teplyakova, E. Y. Obryadina, L. A. Alyoshina, N. A. Evdokimova, and E. P. Feklistova, Crystallogr. Rep. **58** (2013) 541.
32. N. V. Sidorov, N. A. Teplyakova, and M. N. Palatnikov, Opt. Spectrosc. **115** (2013) 685.